

## NCEP NOTES

### A Multigrid Wave Forecasting Model: A New Paradigm in Operational Wave Forecasting

ARUN CHAWLA,\* HENDRIK L. TOLMAN,\* VERA GERALD,\* DEANNA SPINDLER,+  
TODD SPINDLER,+ JOSE-HENRIQUE G. M. ALVES,# DEGUI CAO,@,\*\* JEFFREY L. HANSON,&  
AND EVE-MARIE DEVALIERE&,+ +

\* NOAA/NCEP, College Park, Maryland

+ MSG at NOAA/NCEP, Rockville, Maryland

# SRG at NOAA/NCEP, Camp Spring, Maryland

@ SAIC at NOAA/NCEP, Greenbelt, Maryland

& USACE Field Research Facility, Kitty Hawk, North Carolina

(Manuscript received 25 January 2012, in final form 25 July 2012)

#### ABSTRACT

A new operational wave forecasting system has been implemented at the National Centers for Environmental Prediction (NCEP) using the third public release of WAVEWATCH III. The new system uses a mosaic of grids with two-way nesting in a single model. This global system replaces a previous operational wave modeling suite (based on the second release of WAVEWATCH III). The new forecast system consists of nine grids at different resolutions to provide the National Weather Service (NWS) and NCEP centers with model guidance of suitable resolution for all areas where they have the responsibility of providing gridded forecast products. New features introduced in WAVEWATCH III, such as two-way nesting between grids and carving out selected areas of the computational domain, have allowed the operational model to increase spatial resolution and extend the global domain closer to the North Pole, while at the same time optimizing the computational cost. A spectral partitioning algorithm has been implemented to separate individual sea states from the overall spectrum, thus providing additional products for multiple sea states. Field output data are now packed in version 2 of the gridded binary (GRIB2) format and apart from the standard mean wave parameters, they also include parameters of partitioned wave spectra. The partitioning is currently limited to three fields: the wind-wave component, and primary and secondary swells. The modeling system has been validated against data using a multiyear hindcast database as well as archived forecasts. A new software tool developed by the U.S. Army Corps of Engineers (USACE) is used to extend the analysis from overall error estimates to separate skill scores for wind seas and swells.

#### 1. Introduction

At operational centers like the National Centers for Environmental Prediction (NCEP), numerical models are used to obtain initial forecast guidance that are then used by forecasters who, after accounting for known model errors, issue official forecasts. From a forecaster's

point of view, a valuable model guidance system needs to be (a) as close as possible to the ground truth and (b) delivered in a timely fashion so that it can be used to develop a forecast. Thus, considerable efforts are put in operational centers to improve both model accuracy and computational efficiency. NCEP provides model guidance for wind waves and ocean swells using the third-generation spectral wave model WAVEWATCH III (Tolman 2002c; Tolman et al. 2002; Tolman 2007, 2008, 2009; hereafter referred to as WW3). A typical model configuration for operations uses a third-order propagation scheme that minimizes numerical diffusion (other propagation options are available) and a parallel code was developed to increase computational speed (Tolman 2002a). Until November 2007, the operational forecast

---

\*\* Current affiliation: National Ocean Service, Silver Spring, Maryland.

+ + Current affiliation: NOAA/JCSDA, Camp Springs, Maryland.

---

Corresponding author address: Arun Chawla, NOAA/NCEP, 5200 Auth Rd., Camp Springs, MD 20746.  
E-mail: arun.chawla@noaa.gov

system consisted of a suite of wave models that included a global forecast model (NWW3; Tolman et al. 2002) and three regional models for the Alaskan Waters (AKW; Chao et al. 2003a), eastern North Pacific (ENP; Chao et al. 2003b), and western North Atlantic (WNA; Chao et al. 2003c). Boundary conditions for the regional models were obtained from the global model. This is the classical paradigm of single-grid models with one-way nesting, where locally finer-resolution grid domains are driven as separate models using boundary conditions from the coarser models. Computational costs limited the global operational model at NCEP to a grid of  $1.25^\circ \times 1^\circ$ , and the regional models to a  $1/4^\circ \times 1/4^\circ$  grid. While this resolution is adequate for providing guidance to regional forecasts, coastal forecasts (generated by the various weather forecast offices) are needed at grids with resolutions of 5 km and finer. The one-way nesting paradigm would require that finer-resolution coastal grids be driven as separate modeling systems that could feasibly use data from the regional models as boundary conditions. Running these separate modeling systems can be quite a cumbersome process from an operational point of view. Furthermore, boundary conditions for the regional grids are obtained from the global model, but the finer-resolution effects are not passed back from the regional grids to the global grid.

Since the implementation of the operational wave modeling suites, the WW3 computational model has moved away from a paradigm of representing the domain with a single grid to one where the domain is represented as a mosaic of grids in which there is a two-way exchange of information (from coarser- to finer-resolution grids and vice versa or between grids with similar resolution) (Tolman 2007, 2008, 2009). Using multiple grids within the same model allows for locally increasing resolution to resolve coastal features such as inlets, provide a better representation of the bathymetry for refraction processes in the nearshore region, and at the same time localizes the effects of Courant–Friedrichs–Lewy (CFL) limits on numerical time steps, thus minimizing the computational cost. It should be noted that the biggest advantage of a two-way nested multiple grid paradigm is not the ability to have locally finer-resolution grids (the same can be achieved by a series of one-way nested single-grid models) but that this can be achieved using a single model driver, thus greatly simplifying operational requirements. An additional advantage of a two-way nested paradigm is that this can be the framework for exchanging information across different types of grids (regular, curvilinear, unstructured, etc.), thus having a modeling system that provides flexibility in choosing grids that best fit the local domains (e.g., unstructured grids in coastal waters). Apart from the multigrid approach, the third public release of WW3

also accounts for depth-limited wave breaking, which was absent in the earlier versions of WW3.

The multigrid version of WW3 has been used to develop a new operational forecast system for NCEP. The National Oceanic and Atmospheric Administration (NOAA) Multigrid WaveWatch 3 system (hereafter referred to as NMWW3) has been operational since December 2007 and has replaced the older modeling suite (NWW3, AKW, WNA and ENP). NMWW3 was developed to take advantage of the new features in WW3 with the specific aim of providing finer-resolution forecast guidance without compromising on delivery times. This paper outlines the changes that have occurred in the operational model, both at the computational level and in the generation of products. A detailed validation study of the system (in both forecast and hindcast mode) has been carried out to quantify the skill of this system under varying conditions. The paper ends with identifying the multiple changes that are going to be introduced into the system in the near future.

## 2. WAVEWATCH III upgrades

Many significant changes have been introduced in the multigrid version of WW3 (version 3 and higher) relative to previous model distributions and a more detailed description can be found in Tolman (2008, 2009). Broadly, these changes fall into three categories and a brief overview is provided here.

### *a. Mosaic approach to wave modeling*

In addition to representing a computational domain by single self-contained grids, as was done in the past, the new version of WW3 now allows the domain to be represented by an arbitrary number of grids of different resolutions that can be interconnected via two-way nesting. Grids are ranked according to their resolution, with the coarser-resolution grids having a lower rank, and grids with similar resolution having the same rank. Although each grid acts as a separate wave model, there is now the option of full two-way interaction between the grids in the regions where they overlap. Data for the boundary points of the higher-ranked grids are obtained from the lower-ranked grids that these points lie on, similar to traditional one-way nesting. In the lower-ranked grids, points that lie inside the domain of higher-ranked grids receive spatially averaged data from the latter. This allows sea states that develop in finer-resolution areas to propagate out to coarser-resolution areas. Overlapping grids with the same rank are reconciled in their area of overlap similar to a “halo” approach for domain decomposition in parallel computing.

Data transfer from lower- to higher-ranked grids occurs at defined boundary points. In the classical one-way

nesting approach these points would be along the edges of the grid (Tolman 2002c, see WW3 version 2.22). The new model, however, also allows boundary points to be defined inside the grid, making a distinction between land, active, and excluded points. This feature allows grids to be carved out in arbitrary shapes and has been used extensively in developing an optimal forecast model with coastline-following grids as well as selected domains within the same grid where finer-resolution computations are desired (section 3).

### *b. Partitioning of wave spectra*

Apart from providing guidance on the overall wave height, operational wave forecast models are also used to provide guidance on swell and wind-wave fields to mariners. Traditionally, this has been done by using a frequency and/or a wind-dependent cutoff in the spectrum to separate wind and swell fields. Such a cutoff can partition energy into a swell field even if there are no peaks in the energy spectrum. Furthermore, such an approach cannot separate directionally distinct fields. A new algorithm (Hanson and Jensen 2004; Hanson et al. 2009) for partitioning the energy spectrum has been added to the model. It is based on a digital image processing watershed algorithm (Vincent and Soille 1991) and divides the energy spectrum into partitions based on the number of peaks in the spectrum (in both the frequency and directional domains). Individual peaks are identified as wind seas or swells using an inverse wave-age criterion. This algorithm not only provides a natural way to separate wind seas from swells, but also identifies multiple swell fields in the spectrum.

### *c. New physics*

Two new source terms have been added to the model to better simulate physical processes. One is the linear growth parameterization of Cavaleri and Malanotte-Rizzoli (1981) with a filter for low-frequency energy (Tolman 1992). This term has been added to consistently spin up the model from quiescent conditions, precluding the need for seeding. The second source term is a depth-induced breaking term from Battjes and Janssen (1978) that simulates energy dissipation due to surf zone breaking. This term has been added to extend the applicability of the model into shallow water environments, which has become increasingly necessary with the development of the mosaic approach to wave modeling and the corresponding finer coastal resolution. The source term is based on the criterion that all wave heights exceeding a maximum wave height (depth dependent) in the surf zone will break and the spectral energy dissipation rate is based on the dissipation of a turbulent bore. The model can also now dynamically

switch cells between active and inactive states, using a minimum water depth criterion. This feature is useful for studying the impact of waves in wetting and drying regions when coupled with a surge model like the Advanced Circulation Model for Oceanic, Coastal, and Estuarine Waters (ADCIRC; Luettich et al. 1992) and was used to simulate wave propagation in the marshes of southern Louisiana during hurricane conditions.

## **3. NOAA multigrid forecast model (NMWW3)**

A single operational multigrid forecast model was designed to replace the existing suite of global and regional operational models. The new forecast model was designed to run on the same schedule as the old models, that is, four forecast cycles a day (at 0000, 0600, 1200, and 1800 UTC). Each cycle consists of a 189-h-long run with 9 h of hindcast and 180 h of forecast. Restart files are generated 6 h into the hindcast to be used as starting conditions for the next cycle. The length of the hindcasts was chosen such that initialization for the next cycle is done using the best possible hindcast, because NCEP's final analysis valid for the beginning of the forecast is produced after the wave model has started.

### *a. Grids*

The main aim of developing the NMWW3 model was to provide model guidance for the weather forecast offices (WFOs) and the regional prediction centers (e.g., Ocean Prediction Center and National Hurricane Center) at a suitable resolution within the available computational constraints. The WFOs provide forecasts for the U.S. coastal waters on grids with a 5 km or finer resolution. These grids extend approximately 60 nautical miles (n mi, where 1 n mi = 1852 m) offshore off the U.S. west coast and 40 n mi off the U.S. east coast. The regional forecasts on the other hand are provided on  $\frac{1}{6}^\circ$ -resolution grids by the two prediction centers. The regions that fall under the mandate of regional forecasts include the U.S. west and east coasts, Alaska, Hawaii, the Gulf of Mexico, the high seas region in the Pacific and Atlantic Oceans, and some of the islands in the South Pacific.

To provide appropriate guidance forecasts, the global domain was divided into nine grids:

- two large-scale  $\frac{1}{2}^\circ$  grids (which wrap around the globe along the longitude axis)—two grids have been used to improve computational efficiency at higher latitudes (see details below);
- four regional grids— $\frac{1}{6}^\circ$  grids for the U.S. east coast (includes the Gulf of Mexico and the Caribbean Sea), the U.S. west coast and the Pacific Islands (includes Hawaii and select islands in the Pacific Ocean where

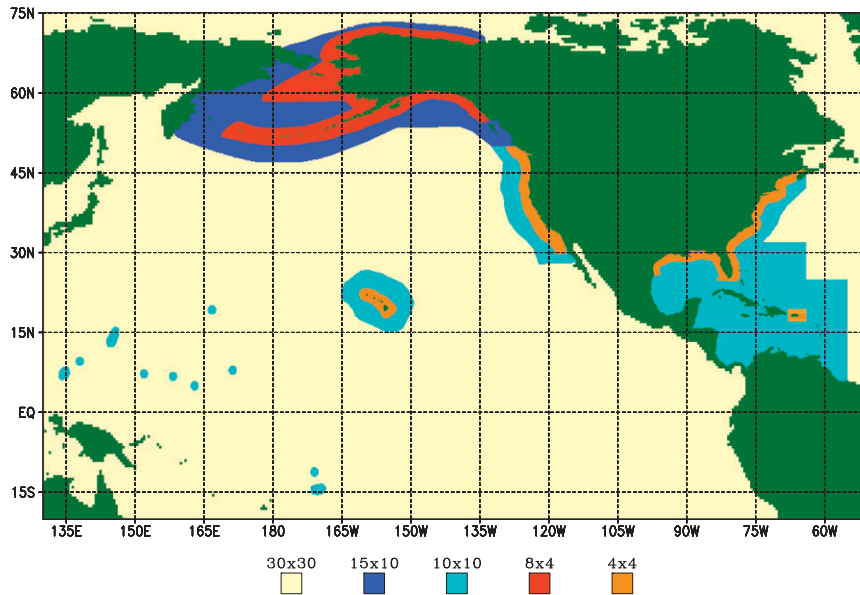


FIG. 1. Grids for NMWW3. Grid resolution is given in arc minutes. Resolutions based on the forecast requirement of the NWS. Note that the global  $0.5^\circ$  grid covers all longitudes and extends from  $77.5^\circ\text{S}$  to  $90^\circ\text{N}$ , with all grid points above  $82^\circ\text{N}$  being marked as undefined.

- the NWS has responsibility for providing forecasts), and a  $\frac{1}{4}^\circ \times \frac{1}{6}^\circ$  grid for Alaska; and
- three coastal grids— $\frac{1}{15}^\circ$  grids for the U.S. east coast (includes the coastal waters of Puerto Rico) and the U.S. west coast (includes the coastal waters of Hawaii), and a  $\frac{2}{15}^\circ \times \frac{1}{15}^\circ$  grid for Alaska.

Figure 1 shows the map representation of the different grids by displaying the highest available resolutions. In contrast, the older models had grid resolutions of  $1.25^\circ \times 1^\circ$  for the global model and  $\frac{1}{4}^\circ$  for the regional models. Separation of the computational domain into nine different grids was done to optimize the parallel implementation within the constraints of desired regional grid resolutions. Note that the coarser-resolution grids extend to the coast, creating a full overlap with finer-resolution grids.

Computationally, the global domain has been separated into two  $\frac{1}{2}^\circ$  grids: a global grid that extends from  $77.5^\circ\text{S}$  to  $77.5^\circ\text{N}$  and an Arctic grid that extends from  $65^\circ$  to  $90^\circ\text{N}$  (the computation however is stopped at  $82^\circ\text{N}$  to avoid the singularities near the pole). This approach was taken so that the CFL time step limitations at higher latitudes are confined to a smaller grid, and was only possible because the two-way nesting algorithm in WW3 allows for the reconciliation and exchange of information across overlapping grids of similar resolution (Tolman 2008). Note that when a domain is described by two grids as opposed to a single grid, the solutions will be different if the two-way communication occurs only

along the boundaries (since the numerical scheme is of the first order at the boundaries and is third order internally). This is circumvented in the modeling system by requiring that grids of similar resolution have a minimum overlapping domain such that the solution from the boundary edge of one grid can be overwritten with the internal solution from the other grid (see Tolman 2008 for details). A long-term solution for modeling waves in the Arctic region is to use a polar curvilinear grid as part of the mosaic of grids. Such an approach is currently under development.

Optimal fine-resolution (in space) regional grids were designed by taking advantage of the model's flexibility in assigning boundary points inside a grid. In the new version of WW3, grid points where finer-resolution results are not needed can be excluded (typically in the open ocean away from the coast). This significantly reduces the number of active points (where model computations are carried out) and the subsequent computational cost. This flexibility allows for efficient coastline-following finer-resolution grids, as seen in Fig. 1. It also accommodates carving out finer-resolution domains from a grid (e.g., Pacific island domains and the region around Puerto Rico in Fig. 1).

The impact of the coastal grids can be clearly seen in simulations of landfalling hurricanes such as Katrina (Fig. 2). The coastline is better represented in NMWW3 and the addition of shallow water wave breaking physics leads to more realistic estimates of wave heights with respect to water depth. It should be noted that the aim of

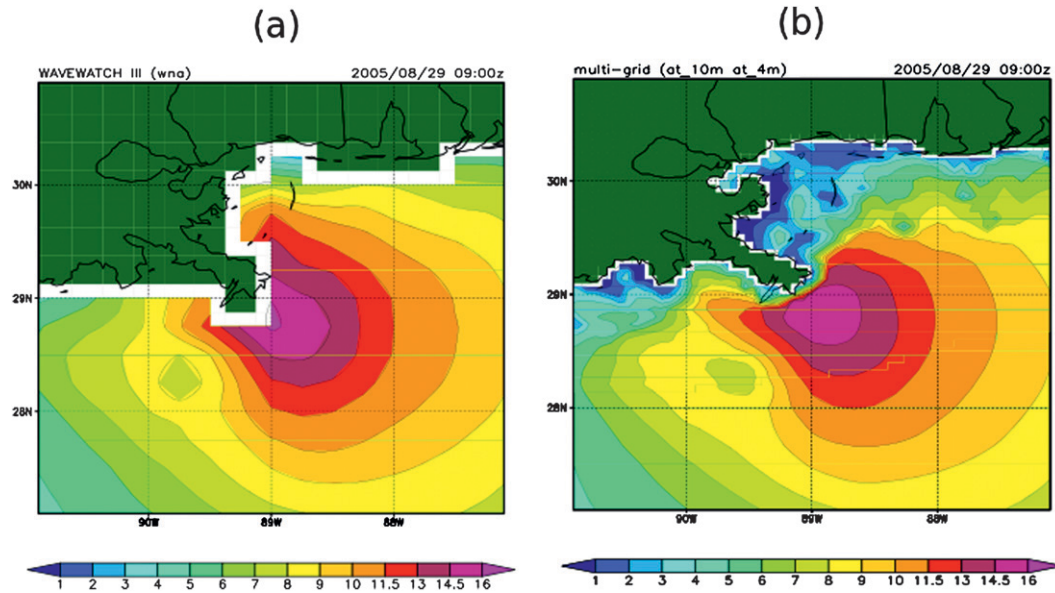


FIG. 2. Significant wave heights (m) during Hurricane Katrina land fall at New Orleans for (a) WNA and (b) NMWW3 models.

these simulations is to only highlight the differences in the WNA and NMWW3 models and as such do not account for the underlying surge that would have a major impact on the wave field of a landfalling hurricane. Coupling of surge models with wave models in operations is part of future implementation plans. The 2' gridded elevations/bathymetry for the world (ETOPO2; NOAA/NGDC 2007) dataset has been used as the reference bathymetry to develop the wave grids. It needs to be noted that even though the modeling system now contains a shallow-water wave breaking dissipation term, the finest grids in the domain still have a resolution on the order of 7 km. That is too coarse to accurately represent the typical surf zone. Furthermore, coastal and bathymetric features (e.g., inlets, shoals, and sand bars) that play a significant role in wave transformations in the nearshore zone cannot be represented in such a system. For nearshore and surf zone dynamics, local fine-resolution wave models [grid resolution  $\leq O(150\text{ m})$ ] with offshore boundary conditions provided by either data or global models such as the present one are more appropriate.

The spectral resolution in NMWW3 follows that of the older models and consists of 29 frequency components and 24 directional components. This yields a directional resolution,  $\Delta\theta = 15^\circ$ . The spectral frequency is discretized following a geometric progression, with an increment factor set at 1.1 (frequency increments by 10%) and the frequency ranges from 0.035 to 0.5. The spectral resolution was recently increased to 50 frequency components and 36 directions ( $\Delta\theta = 10^\circ$ ,

frequency increment factor 1.07) with a frequency range of 0.035–0.96. However, for most of the validation period (section 4), the coarser resolution was used. Comparisons between the finer and coarser resolutions have revealed a very limited impact (figure not shown) of the increased resolution on integrated spectral parameters (such as significant wave height  $H_s$ ). The exception has been some alleviation of the “garden sprinkler effect” under hurricane conditions, which is related to the increased directional resolution (Booij and Holthuijsen 1987). The finer spectral resolution has been introduced primarily for more sophisticated source term packages that will be implemented later. It should be noted that while the original discrete interaction approximation (DIA) is based on a frequency increment factor of 1.1, changing to an increment factor of 1.07 has had minimal impact on the spectra.

#### b. Obstruction model

The algorithm for using obstruction grids to simulate blocking effects from unresolved islands (Tolman 2003) has been an integral part of WW3 since 2002 and remains unchanged in the new version. However, initial grids were developed manually, and in a multigrid model with many grids a manual approach can be tedious and onerous. Furthermore, due to the two-way coupling of the grids, the obstruction grids need to be consistent across grids in the regions of overlap. In a manual approach where the choices are subjective, this is not guaranteed. To alleviate these concerns, an automated grid generation package was developed for WW3

(Chawla and Tolman 2007, 2008). In this package obstruction grids are generated using the Global Self-Consistent Hierarchical High-Resolution Shoreline (or GSHHS) database (Wessel and Smith 1996). The software for grid and obstruction generation is provided with the public distribution of the wave model (model version 3.14, available for download online at <http://polar.ncep.noaa.gov/waves/wavewatch/wavewatch.shtml>).

### c. Forcing fields

The wave model is forced by 10-m (above MSL) winds, air-sea temperature differences, and ice concentration data. In the single-grid version of WW3, forcing data needed to be on the computational grid. In the multigrid version, forcing data can be defined on their own unique grids (data are interpolated or averaged from the forcing grid to the computational grid internally in the code) or be defined on the computational grids. The former approach is used in NMWW3 as it precludes the need to develop individual forcing files for each grid as well as maximizing the consistency of winds across the different grids and scales. Sea ice concentration data are updated once a day over a global  $1/12^\circ$  grid using an automated passive microwave analysis (Grumbine 1996). For a particular forecast, sea ice is kept constant. Forecast winds are obtained from the Global Forecast System [GFS, previously known as the Aviation Model/Medium-Range Forecast model (AVN/MRF); Kanamitsu (1989); Kanamitsu et al. (1991); Caplan et al. (1997)]. Hindcast winds are obtained from the Global Data Assimilation System (GDAS; Kanamitsu 1989; Derber et al. 1991), which uses global observations to provide the initial conditions for the GFS model. Apart from the hindcast winds, GDAS is also used to determine the initial sea surface temperature, which is based on an analysis of ship, buoy, and satellite data (Reynolds and Smith 1994). This is then kept fixed through the forecast. All the wind data are provided at 3-h intervals. Wind data are obtained from the lowest sigma level ( $\approx 20$  m above MSL) of the atmospheric model on a  $1/2^\circ$  spatial grid and converted to 10-m winds assuming a neutrally stable vertical boundary layer.

Since the interpolation of wind fields is done internally for each grid (and is not a part of the preprocessing), NMWW3 was designed so that it can run side by side with the GFS model. Taking advantage of the modular nature of WW3, the modeling system was reconfigured so that the model could be run either in “once through” or a “side by side” option. The former is the classical approach where the model proceeds through the forcing file till the end of the run. In WW3 if the forcing wind data ends before the end of the run, the wind information from the last input is used for the remainder of the run. However, when

the model is run using the side-by-side option, if the end of the wind file is reached before the end of the run, the model pauses till the wind file is updated. This is the approach used in operations. This way, the model can be started soon after the GFS model and run side by side with the latter. There are several advantages to such an approach. First, model output is available shortly after the GFS data are ready (as opposed to the earlier practice of waiting for the GFS model to complete 180 h of a forecast before launching the wave modeling suites), significantly improving the delivery times of guidance products. This also has the added benefit of both wave and wind information being delivered nearly concurrently to the forecasters. Second, since the GFS model is computationally more intensive, this allows the wave model to run using a smaller number of resources than would be necessary if the model was launched after the GFS model had completed generating all the forcing files. Finally, this sets the stage for true coupling between the wave model and the atmospheric model, to be pursued in the future.

### d. Outputs

There are two types of output data in NMWW3: field data and point data.<sup>1</sup> This is similar to the output fields of the older wave models. However, there are some differences.

Field data consist of the integral parameters of the ocean spectral data represented on a spatial domain (Table 1). Field output data are available on the same grids as the computational grids. For computational reasons, the global domain was split into two overlapping  $1/2^\circ$  grids, which do not need to be maintained separately for outputs. Thus, the outputs from these two grids are combined and field output data are provided over eight grids (with the global  $1/2^\circ$  grid extending from  $77.5^\circ\text{S}$  to  $90^\circ\text{N}$ ). The same field outputs that were part of the old operational models are also available in the new model. However, the new model also includes a partitioning algorithm that separates a 2D spectrum at all active grid points into individual sea states. The sea states are separated into wind seas and swells, with the spectral parameters of each sea state being part of the output.

The wind wave portion of the spectrum is given by a single component, even if the spectrum in this region has multiple peaks. The partitioning algorithm does not put a limit on the number of possible swell fields in the spectrum. However, in the operational model, output is

---

<sup>1</sup> All output products generated by the operational wave model are identified as NOAA WAVEWATCH III, which is a registered trademark of NOAA.

TABLE 1. Spectral parameters output on the computational grids. Data are output in GRIB2 format, with a separate file for each computational grid and output time. All directions use the meteorological convention (direction from using compass notation with 0° corresponding to true north). Partitioned data (wind seas and swells) parameters are only computed over the partitioned segment of the spectrum with the data being marked as undefined if either no partition is found or the significant wave height is below a cutoff limit (set at 10 cm). Note that for swells there are two sets of output parameters corresponding to primary and secondary swells. Swell significant wave height is used as a criterion to separate waves into primary and secondary swells.

Name	Unit	Description
WIND	m s <sup>-1</sup>	Wind speed (interpolated from wind grid)
WDIR	°	Wind direction
UGRD	m s <sup>-1</sup>	<i>U</i> component of wind
VGRD	m s <sup>-1</sup>	<i>V</i> component of wind
HTSGW	m	Significant wave height (over the full spectrum)
PERPW	s	Peak period
DIRPW	°	Mean wave direction at peak period
WVHGT	m	Significant wave height of wind waves
WVPER	s	Peak period of wind waves
WVDIR	°	Mean wave direction at peak period of wind seas
SWELL	m	Significant wave height of swells
SWPER	s	Peak period of swells
SWDIR	°	Mean wave direction at peak period of swells

currently limited to the first two swell fields, which are referred to as the primary and secondary swells (swell fields are ranked by significant wave height). Figure 3 shows a spatial map of significant wave heights from the overall spectrum as well as from the individual partitions. The white spaces indicate that there is no energy in that partition. For example, in Fig. 3, off the coast of Alaska (45°N, 150°W), the high seas are identified as purely wind seas (since there are no corresponding swell fields). Away from the largest waves, the wave field transitions from wind seas to swell fields. There are several additional locations of pure wind seas. In other areas the seas are a mixture of swells and wind seas. Products such as these are useful to forecasters, as swells and wind seas represent different safety hazards to mariners. Partitioning is done locally over the 2D spectrum at each grid point and output time step.

Field data in NMWW3 are packed using the GRIB2 standard format from World Meteorological Organization (WMO), which provides greater flexibility in metadata handling and more efficient packing options than the earlier GRIB standard (which is used in the older modeling suites). To allow for future increases in the number of output swell fields, swell parameters are stored as vertical levels, with the first level corresponding to the

primary swell. Field output is also now generated side by side with the model run (and not at the end as was done earlier), and made available within shorter delivery times.

Like the older forecast model suites, point output data in NMWW3 provide both detailed spectral data as well as the mean spectral characteristics. Since in NMWW3 a point location can be in multiple grids, the data are automatically retrieved from the highest-ranked grid (highest resolution) that the point lies on. As before, the list of points includes current and old buoy locations and virtual buoy locations, as well as boundary locations (for collaboration projects within and outside NOAA using NMWW3 results as boundary conditions for external models). This list has been expanded to include buoy points from several agencies around the world that maintain wave observation platforms.

#### 4. Validation

The NMWW3 model has been in operations since December 2007. As part of operations, a daily archive of select model results (at collocated altimeter and buoy locations) is maintained. Apart from that, a database of hindcast runs (using NMWW3 settings) extending from February 2005 to the present has been developed and is maintained. Both the archived forecasts and the hindcast datasets have been used to obtain a baseline global skill assessment of the multigrid model. The study spans several years to look for seasonal trends.

##### a. Altimeter comparisons

For altimeter comparisons, the *Jason-1* satellite data have been used to provide estimates of the significant wave height,  $H_s$ . The altimeter data used are the so-called fast-delivery data, which are available in near-real time. Error metrics have been computed using month-long records of the daily forecast archive to ensure global coverage. Calibration and validation of the fast-delivery satellite data with buoy measurements was done by Tolman et al. (2006), and a minor linear bias correction is applied to the satellite data. As part of this study, these calibration curves were confirmed using the 2008 altimeter dataset (figure not shown).

A despiking algorithm is used to remove spikes in the altimeter data. The despiking algorithm also accounts for islands that lie along the altimeter track (but are too small to be resolved in the model domain). A running average is used to smooth the altimeter data.

Figure 4 shows the error metrics (scatter index and bias) computed using raw and averaged altimeter data as a function of the forecast period. The scatter index (SI) is given by

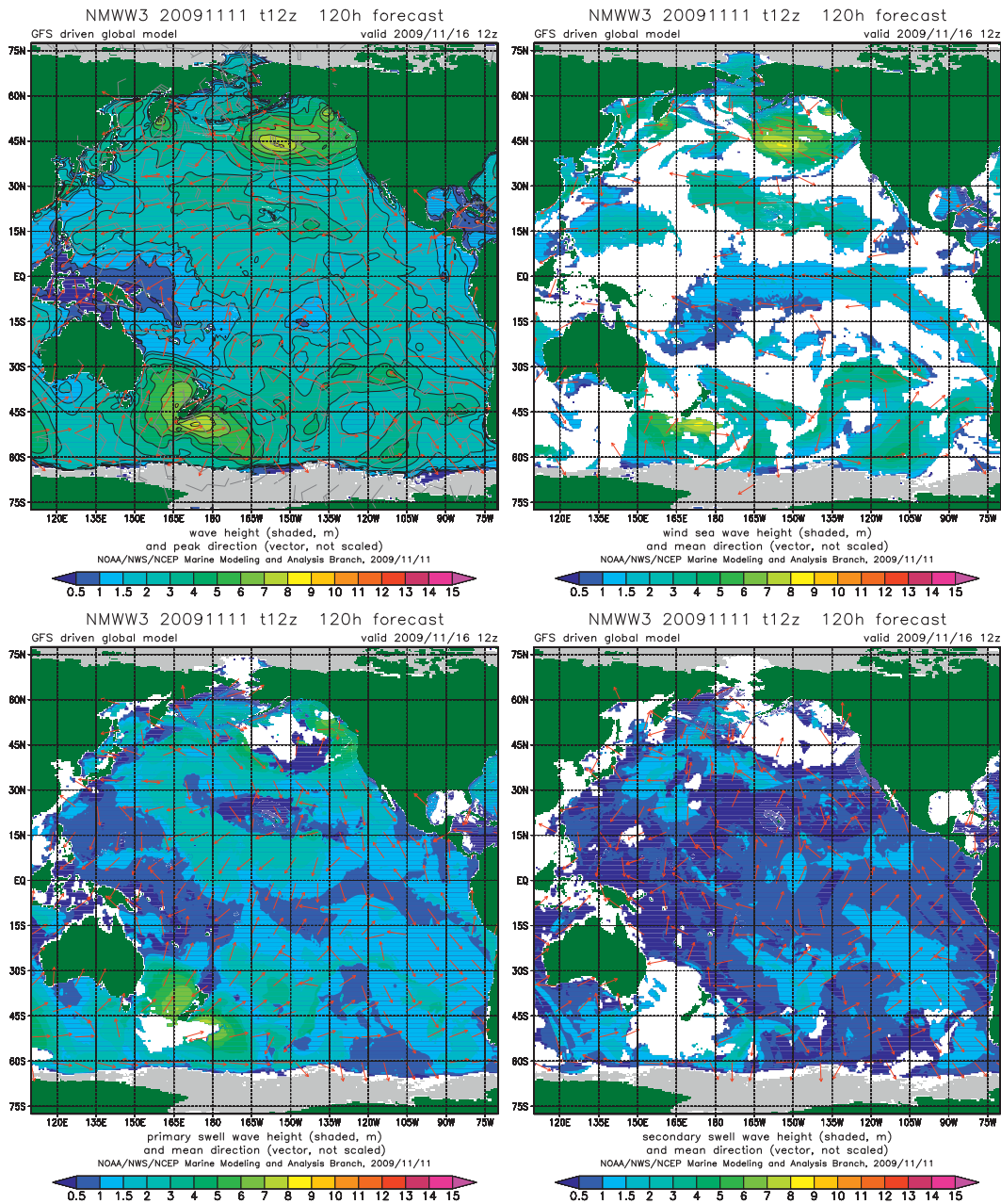


FIG. 3. Snapshot of the spatial distribution of significant wave height (top left) computed from the overall spectrum as well as (top right and bottom) the separate partitions. For the partitioned data if the wave height is below a cutoff limit (currently set at 5 cm in the model), then it is marked as undefined. This accounts for the white spaces in the maps.

$$SI = \frac{\sqrt{\sum(y_m - y_o)^2 - [\sum(y_m - y_o)]^2}}{\sum y_o}$$

where  $y$  is the variable for which the error metric is being computed and the subscripts  $m$  and  $o$  refer to the model and observations, respectively. Since there are multiple grids in the model, the metrics are computed over different domains (as shown in Fig. 4). Overall, there is

a significant difference in SI when using raw as opposed to averaged data but not much difference between the three different levels of averaging (7-, 11-, or 15-point averaging). The 15-point averaging corresponds to a  $\sim 1/2^\circ$  sampling box for the *Jason-1* satellite data (sampling interval 1 Hz), which is equivalent to the coarsest grid resolution in the model. Thus, for the remainder of the paper, comparisons have been made with the 15-point smoothing applied to the altimeter data.

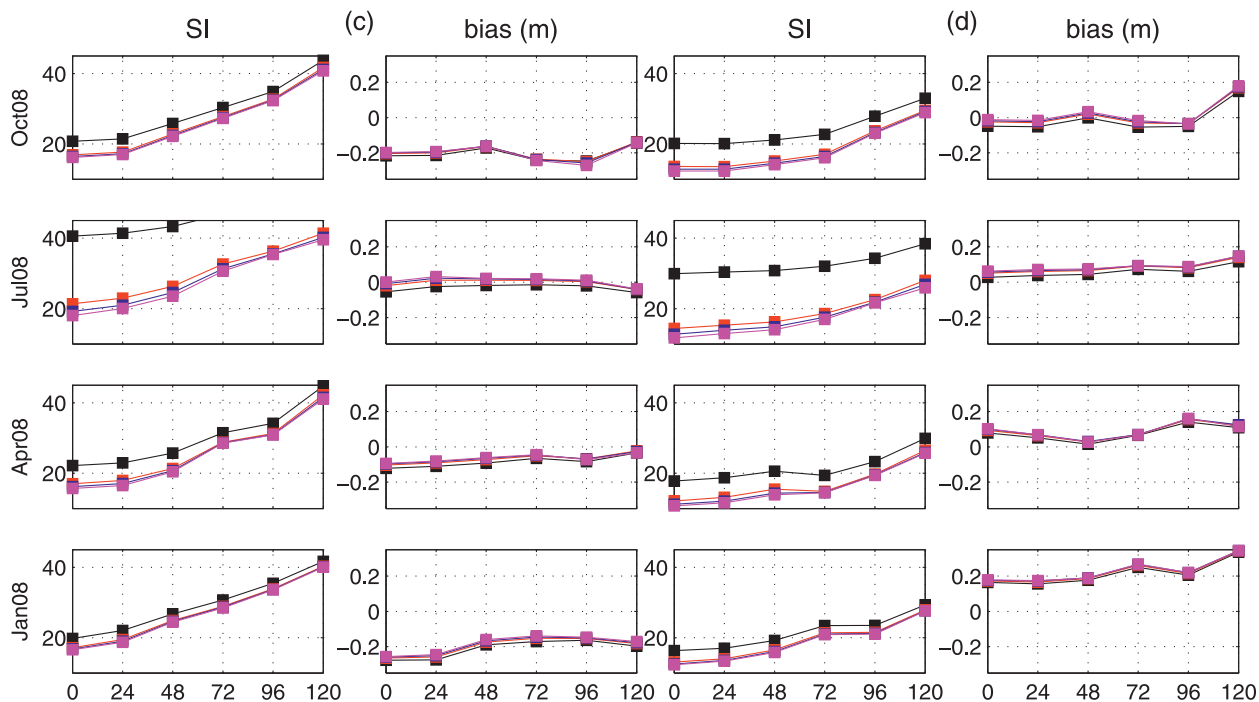
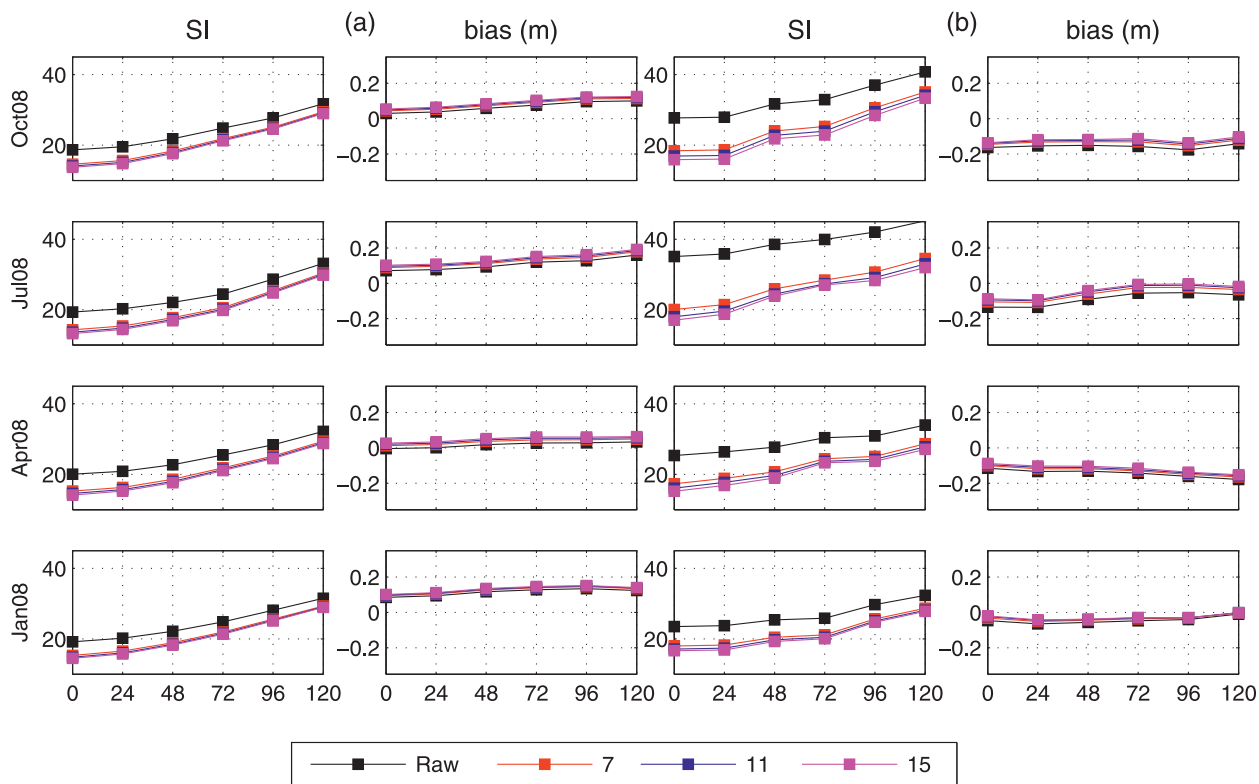


FIG. 4. Error metrics of significant wave heights from the altimeter data as a function of forecast hour for four different months: (a) global domain and (b) Atlantic, (c) Alaska, and (d) Pacific regional domains. The regional domains refer to the 10-arc-min grids shown in Fig. 1. Different lines correspond to different levels of smoothing applied to the altimeter data.

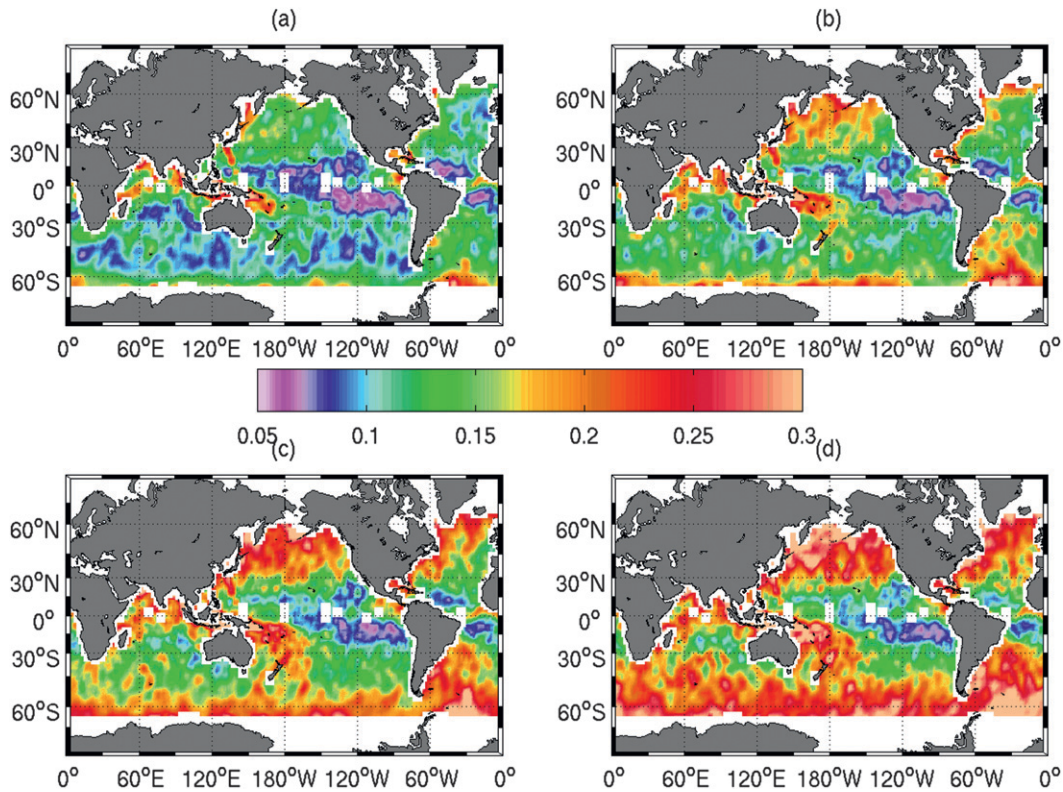


FIG. 5. SI map of significant wave heights for different periods of the forecast cycle. Map is generated by binning collocated model and altimeter data into  $2^\circ \times 2^\circ$  bins. Collocated data from January through March 2008 are used to provide enough points per bin for statistical analysis. A three-point running average along the latitudes and longitudes is also applied to remove the signature of the tracks. Shown are (a) the hindcast and the (b) 48-, (c) 72-, and (d) 96-h forecasts.

The SI relative to smoothed altimeter data does not show any seasonal variations (there is more evidence of this in the buoy comparisons later in the paper) and grows slowly over the first 48 h of a forecast and faster after that. Because the wave model represents a forced and damped system, this error growth represents the error growth in the forcing (GFS). Plots of wind speed error metrics bear this out (figure not shown here). On the other hand, the bias estimates (Fig. 4) show a seasonal variability, and this variability manifests itself differently in different domains. Just like with the SI, the bias increases as a function of forecast hour, albeit much more weakly.

Spatial maps of indices (Fig. 5) show that in general SI increases with forecast time in storm tracks at higher latitudes, but not in swell-dominated areas (e.g., tropics). Again indicating a greater uncertainty in wind sea forecasting than in swells, probably because swells depend less on forecast winds and more on analysis winds. Since the bias shows a stronger variation as a function of season than of forecast hour (Fig. 4), bias maps were created only for the hindcasts and for different times of the year (Fig. 6).

The bias maps show the seasonal variability that was alluded to in Fig. 4. In the Northern Hemisphere, during the winter months there is a positive bias in the swell-dominated parts of the ocean basins (the Pacific and to a lesser degree the Atlantic), indicating that these are probably related to the dissipation in swells (Ardhuin et al. 2009). The western part of the basins shows a persistent negative bias. There is also a persistent positive bias over large regions in the Southern Hemisphere that will be discussed in section 5.

#### b. Buoy comparisons

The buoy data used in the comparison are obtained from a central archive of bulk spectral parameters from over 250 buoys all over the world that is being maintained by the European Centre for Medium-Range Weather Forecasts (ECMWF) as part of a data exchange program (Bidlot et al. 2007b). The hourly buoy data have been averaged over a  $\pm 2$  h interval centered at the four synoptic time cycles (0000, 0600, 1200, and 1800 UTC) at which model forecasts are run. Processing and quality control of these data are done at ECMWF.

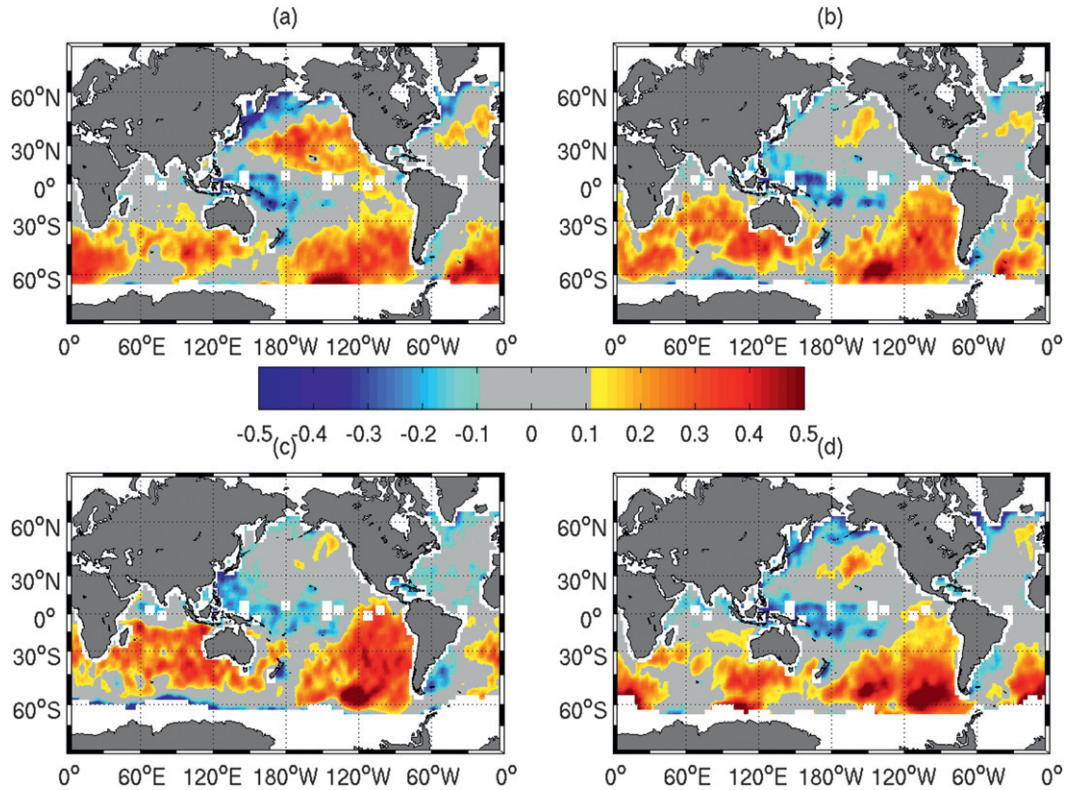


FIG. 6. Bias maps of significant wave height hindcast simulations (m) during different times of the year during 2008. Bias maps are generated in the same way as the SI maps (see Fig. 5 caption for details). Time periods shown are (a) January–March, (b) April–June, (c) July–September, and (d) October–December.

Figure 7 shows the locations of the different buoys. For the purposes of analysis in this paper, the buoys have been grouped by region. The error metrics for the different regions as a function of time can be seen in Fig. 8. The seasonal biases that were alluded to in the altimeter comparisons can be clearly seen in the time series plots, with the wind sea (swell) dominated regions showing a negative (positive) bias during the energetic winter months. The development of the persistent positive bias in the Southern Hemisphere can be clearly seen. SI computations do not show much of the seasonal trend identified in the bias plots and tend to be fairly low everywhere, growing with the forecast hour. Like the altimeter data, buoy data also show the tendency for the indices to be larger in areas dominated by wind seas as opposed to swells. The overall RMS errors show strong correlation with the bias patterns, indicating that a significant part of the total error comes from the model biases.

### c. Spectral comparisons

The limitation of spectral analysis is that it is difficult to develop quantifiable skill metrics. Hanson et al. (2009) have developed a spectral analysis package (the Interactive Model Evaluation and Diagnostics System,

or IMEDS) to address this. This package is used here to gain further insights into the skill of NMWW3.

IMEDS uses the same partitioning algorithm that is currently in WW3 to identify individual wave components in a 2D (or 1D) wave spectrum, which are then separated into wind seas and swells.<sup>2</sup> To ensure a one-to-one correspondence, model spectra are interpolated at the same frequency resolution as the data. Partitions are determined from the data, and within each partition the standard bulk spectral parameters are used to compute error metrics. To avoid the uncertainty associated with identifying spectral peaks, there is the option of using the second moment period  $T_{m02}$  defined by

$$T_{m02} \equiv \sqrt{\frac{\int S(f, \theta) df d\theta}{\int f^2 S(f, \theta) df d\theta}}$$

<sup>2</sup> Since buoy data do not provide a true 2D spectrum, directional information when available is only used for mean direction in this paper.

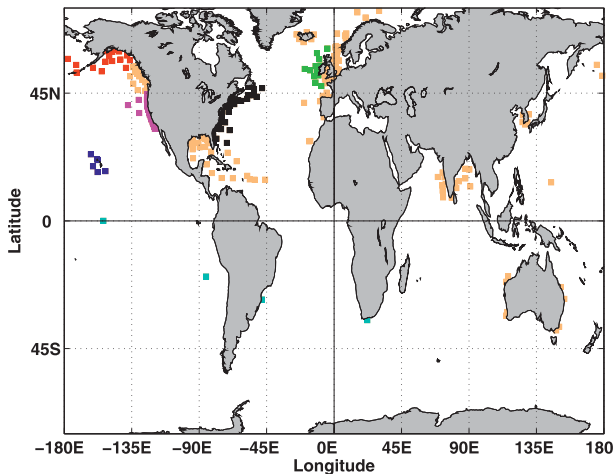


FIG. 7. Locations of buoys used in computing the error metrics. Map shows all the buoy locations where data are available. Buoys were grouped according to region to compute error metrics. The buoys making up the regions in Fig. 8 are color coded as follows: red = AKW; magenta = West Coast; black = East Coast; blue = HI; green = Europe; and cyan = Southern Hemisphere.

IMEDS comparisons were done using select National Data Buoy Center (NDBC) buoys along the Atlantic and Pacific coasts (Fig. 9). The analysis was carried out using the hindcast database, and for simplicity was separated into year-long segments. Error metrics (at any particular buoy in a given year) were computed over month-long segments. Results across different years were fairly similar and thus results from only 2008 are shown here. The buoys were grouped as either coastal or offshore based on their distance from the coast. For brevity only the error metrics from the coastal buoys are shown. The metrics from offshore buoys, with minor exceptions, were very similar.

### 1) ATLANTIC BUOYS

In general the wind seas show a negative bias in  $H_s$  (Fig. 10) during the winter months, similar to the seasonal bias patterns seen in Fig. 8. The swell fields (particularly the young swells) show both negative and positive biases. The negative bias (in  $H_s$ ) in the wind seas during the winter months is larger in the coastal buoys than the offshore buoys with the exception of one buoy (figure not shown), in accordance with the bias patterns seen in Fig. 6. The SI also reduces as we move from the coastal buoys, which are in an area of active wave generation to the offshore buoys. Wave height biases were also plotted as a function of direction for those buoys with directional data (Fig. 11). The biases tend to be more negative when the waves are propagating from the land.

The bias in  $T_{m02}$  (Fig. 12) is negative at most buoy locations (with the error being on the order of 1 s). This

is expected as the DIAs in WW3 are slower in transferring energy from the higher to lower frequencies. Spectral plots at some of the coastal stations (figure not shown) show a bimodal spectra with a second peak between 0.2 and 0.3 Hz in the data that is not reproduced by the model. This is probably driven by local wind processes that are not well reproduced by the coarser global atmospheric model and explain some of the positive biases in  $T_{m02}$  observed.

### 2) PACIFIC BUOYS

The  $H_s$  biases on the Pacific Ocean (Fig. 13) are almost always positive, consistent with our previous analysis (Figs. 6 and 8). This overall positive bias is driven primarily by the positive biases in the swell fields. The wind seas continue to show the negative biases seen in the buoys on the Atlantic Ocean. Since individual swells are not being tracked as they propagate across buoys spread over the Pacific basin, the biases were also separated by their direction (Fig. 14). The biases are highest for waves that are propagating directly from the west (longer swell propagation distance), indicating that the swell dissipation process (Ardhuin et al. 2009) is not adequately simulated in the wave model. Interestingly, in the wind seas, biases as a function of direction are not as clear as they were in the Atlantic buoys. This is probably because we have much fewer instances of wind seas blowing from the coast.

In  $T_{m02}$  (Fig. 15) the biases are generally positive (as opposed to being negative for the Atlantic buoys), most probably because of the higher energy in the lower-frequency components in the wave model due to the absence of swell dissipation. There are instances in swell conditions when the spectral peak frequency of the wave model is lower than that of the data (figure not shown here), but this is not always the case.

## 5. Discussion

Validation studies of NCEP's wave modeling system using WW3 highlight three main points:

- (i) Swell fields are overestimated in the wave model, with the biases being larger in the systems propagating large distances.
- (ii) There is an underestimation of wind seas, particularly in short fetches.
- (iii) There has been a growth in wave biases in the Southern Hemisphere since 2005.

Wave height biases make up a large proportion of the overall error in the wave model, and being able to effectively reduce them will lead to a strong improvement in the model performance. Some of the larger biases are

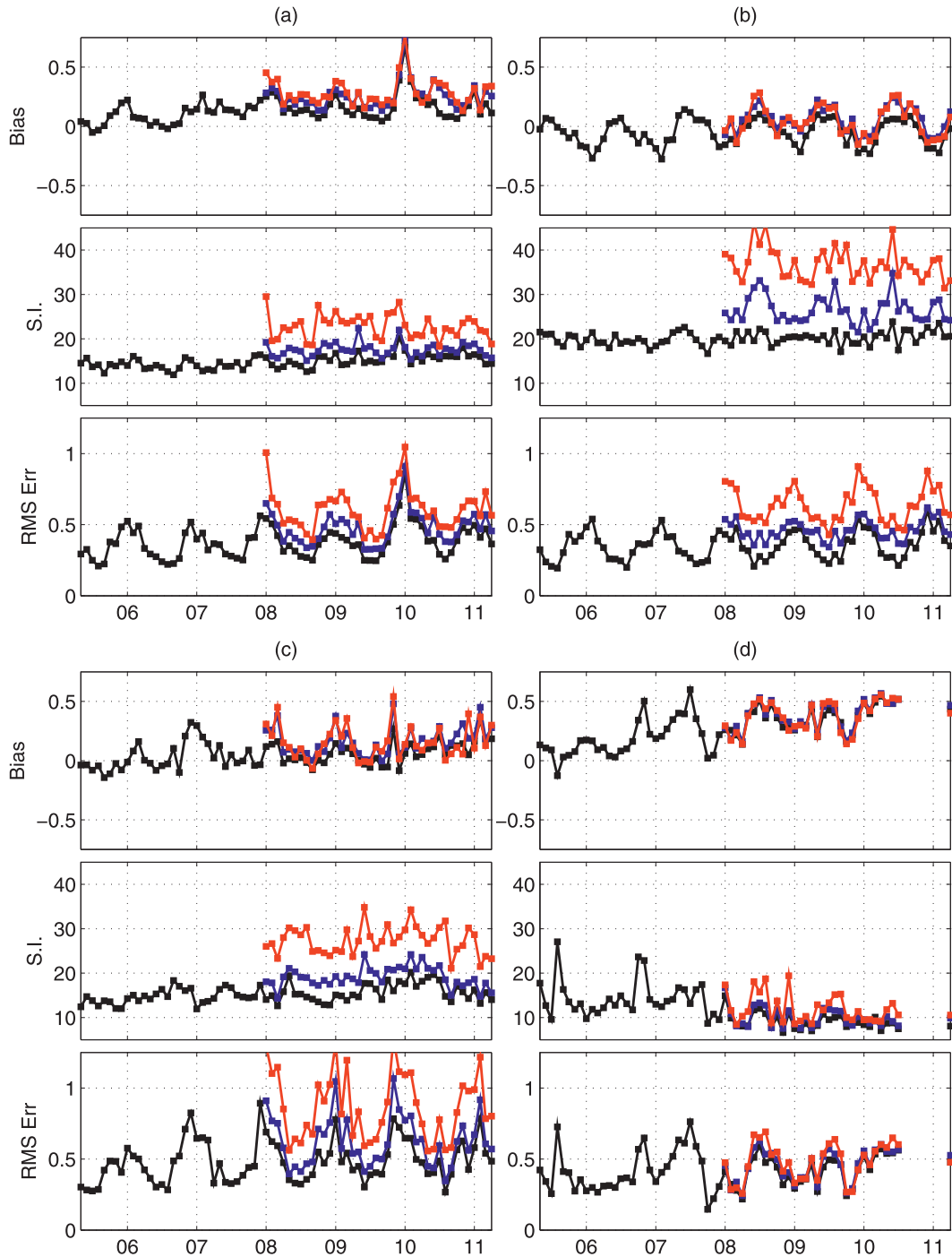


FIG. 8. Error metrics of significant wave heights at buoys (m). Here, black is used to indicate wave hindcasts, and blue and red are for, respectively, 48- and 96-h forecasts. Buoys are from the (a) West Coast, (b) East Coast, (c) Europe, and (d) the Southern Hemisphere. Map showing the buoy locations for each region is given in Fig. 7. Each error metric is computed for a month-long record over all the buoys in the region. Forecast data only are available since the model moved to operations.

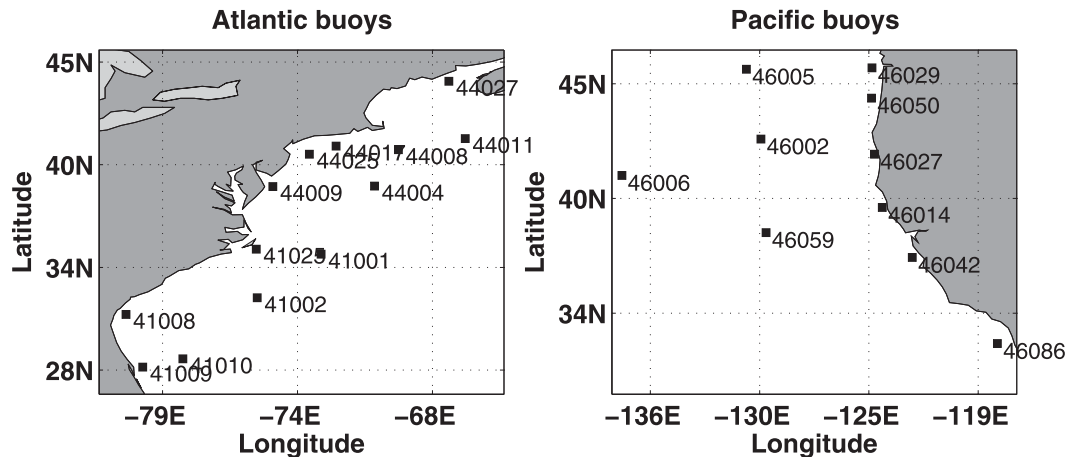


FIG. 9. NDBC buoys used in the IMEDS analysis.

due to a lack of effective swell dissipation in the wave model. The operational wave model uses the physics packages from Tolman and Chalikov (1996). That package gets its wind input term from Chalikov and Belevich (1993), which includes a negative term for waves propagating faster than the wind speed. This negative input term essentially acts as a swell dissipation term and was tuned to fit data as part of WW3 validation studies (Tolman 2002d). Hence, swell dissipation was always part of the model. However, in the absence of any measurements, this was strictly a tuning parameter that was used to reduce the overall error in the wave model. Measurements by Ardhuin et al. (2009) have shown this to be a nonlinear process that is a function of wave steepness.

The weaker swell dissipation in turn has an impact on wave growth. It has been known for some time that in short fetches the wind input term in WW3 underestimates wave growth (Rogers 2002; Ardhuin et al. 2007). This is compensated for by weaker dissipation in transition and swell regions, and is manifested as negative biases in wind seas that reduce with increasing fetch.

With the development of an appropriate swell dissipation source term that can simulate the energy decay for wave systems that propagate long distances, the wind wave growth term can be made stronger to reduce the overall errors. A new source term package has been developed by Ardhuin et al. (2010) that combines the stronger wave growth physics in the work of Janssen (1991) and Bidlot et al. (2005, 2007a), coupled with new terms for dissipation due to wave breaking that take into account the advances made over the last decade in understanding the underlying physical processes (Banner et al. 2000; Song and Banner 2002; Banner and Song 2002; Young and Babanin 2006; Banner and Peirson 2007), as well as a new swell dissipation source term

based on the observations of Ardhuin et al. (2009). The source package has been tested at NCEP using the operational settings and reduced overall errors by  $\sim 30\%$  when compared to current operations (Tolman et al. 2011). The error reduction occurs in both the persistent (bias) and random (SI) errors. The new package went into operations in May 2012.

Apart from the seasonal biases seen in the Northern Hemisphere, there has also been a persistent positive bias over large regions of the Southern Hemisphere that was observed in the bias maps from the altimeters (Fig. 6) as well as time series comparisons at the buoys (Fig. 8). This was surprising because these biases have increased considerably in comparison to the older NWW3 model (Tolman 2002d,b). Tests with the old model setup (figures not presented here) confirm that this shift in bias patterns is not due to the changes to the new model setup and have crept into the model since 2006 (Fig. 8).

A possible reason for persistent increased biases in the Southern Hemisphere is that the representation of the winds in this region by the GFS model has changed since the last time that the wave model was tuned. Figure 16 shows the wind statistics (from the GFS model) over water in both the Southern and Northern Hemispheres. Since 2005, we can see a clear upward shift of the higher wind speeds in the Southern Hemisphere that coincides with the increase in wave biases in the Southern Hemisphere. It needs to be pointed out that the change in GFS forcings in the Southern Hemisphere does not mean that the atmospheric forcings have degraded in quality (in fact, studies being done for a separate publication indicate the opposite), just that the tuning of the wave model was done in a different wind regime.

While the increase in biases does correspond with an increase in wind speeds in the Southern Hemisphere, these winds are not stronger than the ones observed in

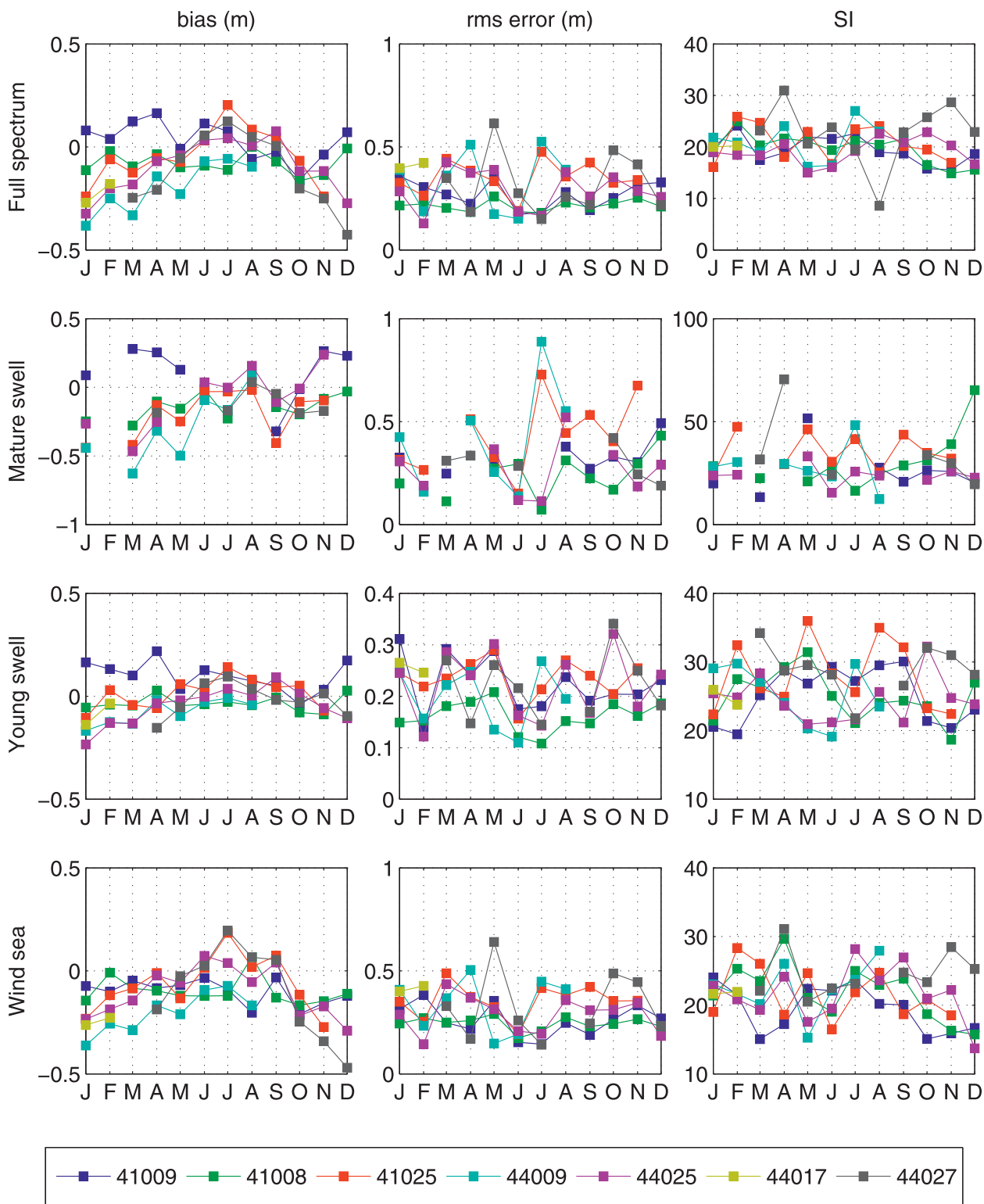


FIG. 10. Significant wave height error metrics from IMEDS for the Atlantic buoys during 2008.

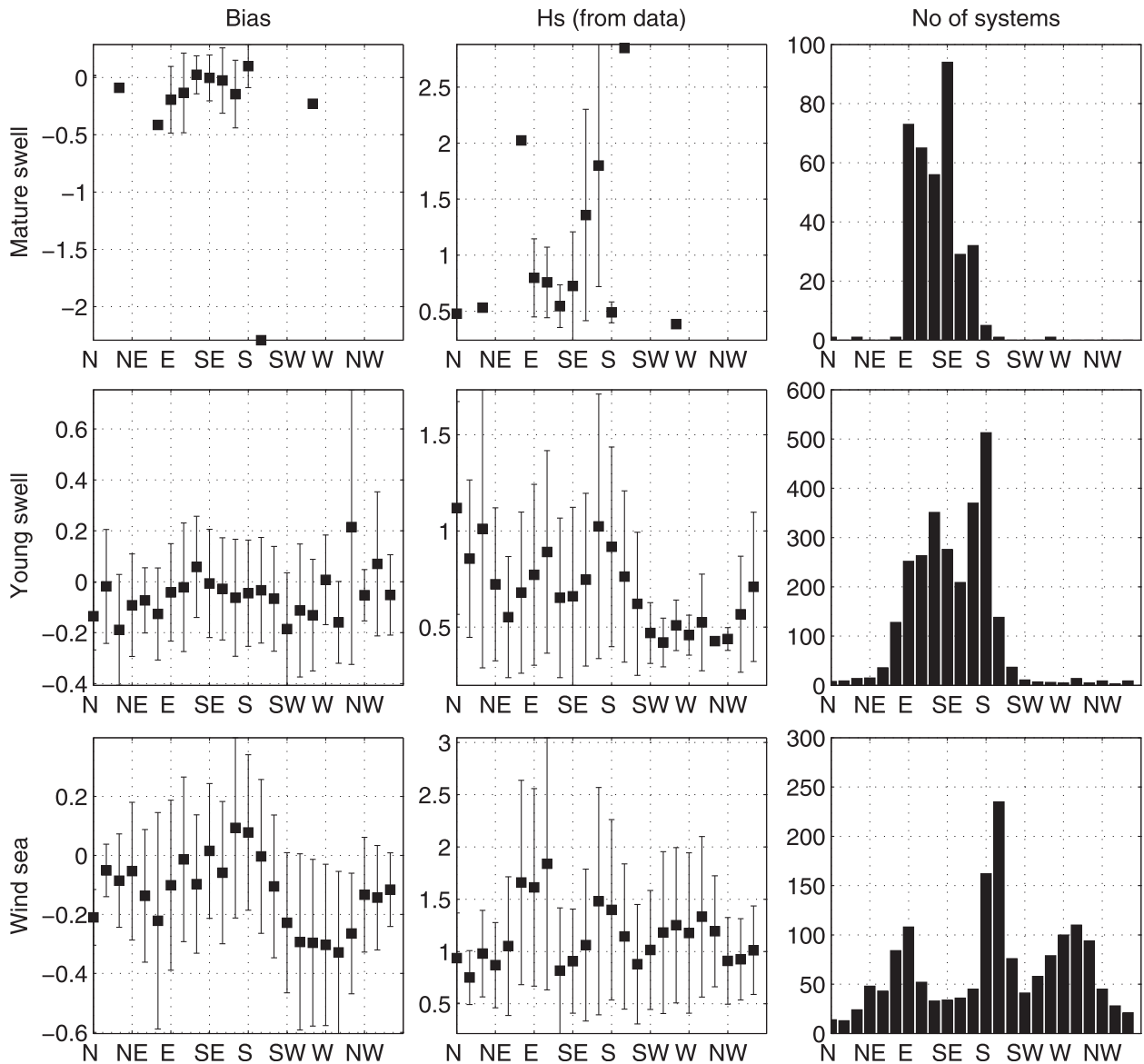


FIG. 11. Significant wave height bias as a function of direction at buoy 44025. Directions refer to the directions from which the waves are propagating. At each buoy data are binned in  $15^\circ$  bins for the entire year. For each buoy mean bias, the average wave height and number of wave systems are plotted as a function of direction. Error bars indicate the standard deviation in a particular bin. In general the spread is larger when the number of samples is small.

the Northern Hemisphere. A possible explanation for the higher (than expected) wave biases is the role played by icebergs in blocking waves. Ardhuin et al. (2011) have shown that the icebergs have a significant impact on wave biases in the Southern Hemisphere. They have shown that the iceberg distribution has an interannual variability, with considerably larger iceberg volumes in 2004 and 2005, as well as 2008, which can have a significant impact on wave biases in the Southern Ocean. The impacts of these icebergs were probably masked by the weaker GFS winds (and, possibly, a smaller number of

icebergs) when the model was being tuned in 2001.<sup>3</sup> The weaker (than observed) swell dissipation in the wave physics further exacerbates this process, and using the new physics package reduces some of these biases (Tolman et al. 2011). Another process that can impact wave biases in the Southern Hemisphere is the wave–current interactions between the waves and the Antarctic Circumpolar Current (ACC). Since this current moves in the direction of the

<sup>3</sup> Our thanks to the reviewers for bringing this to our attention.

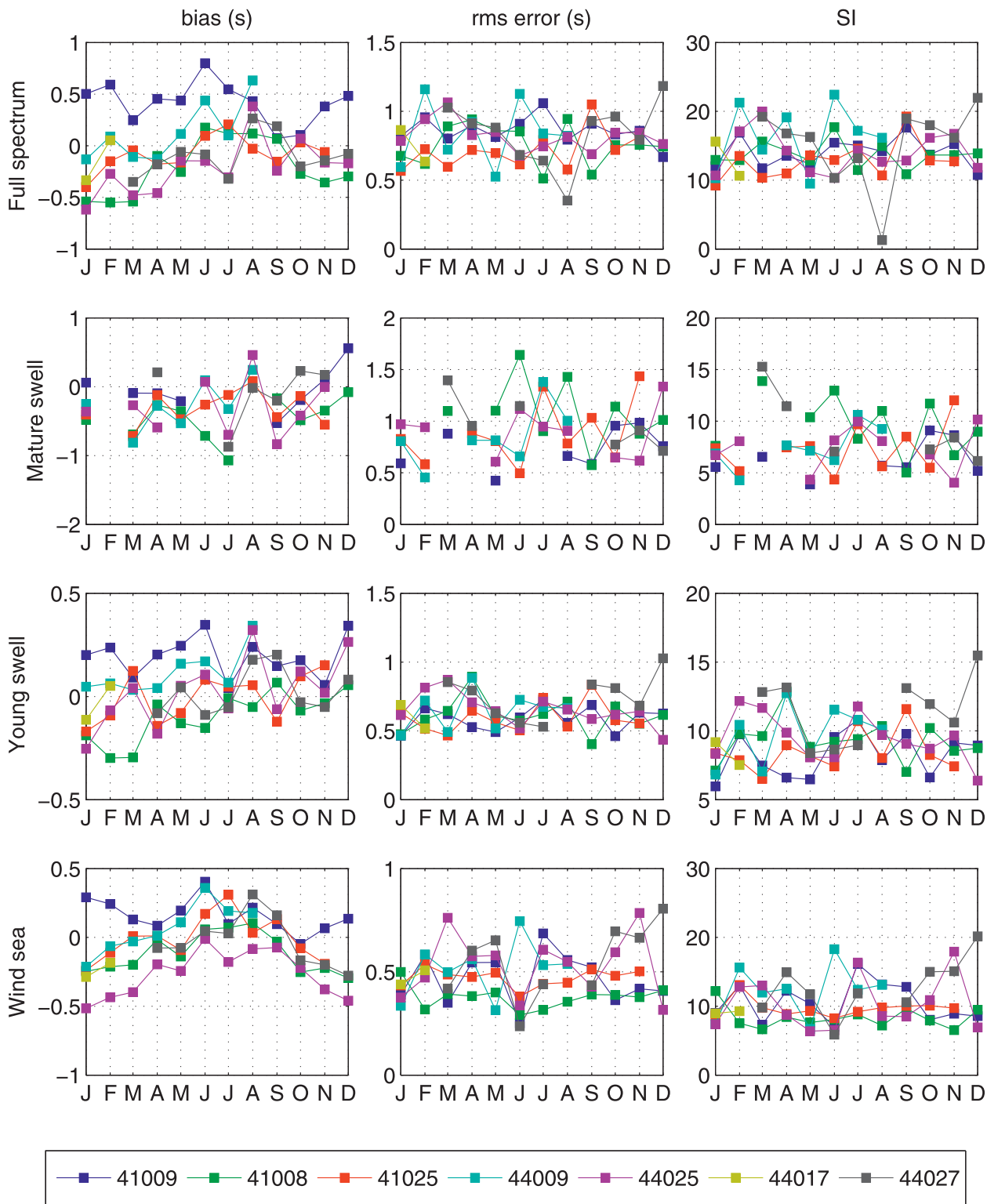


FIG. 12. Wave period error metrics from IMEDS for the Atlantic buoys during 2008.

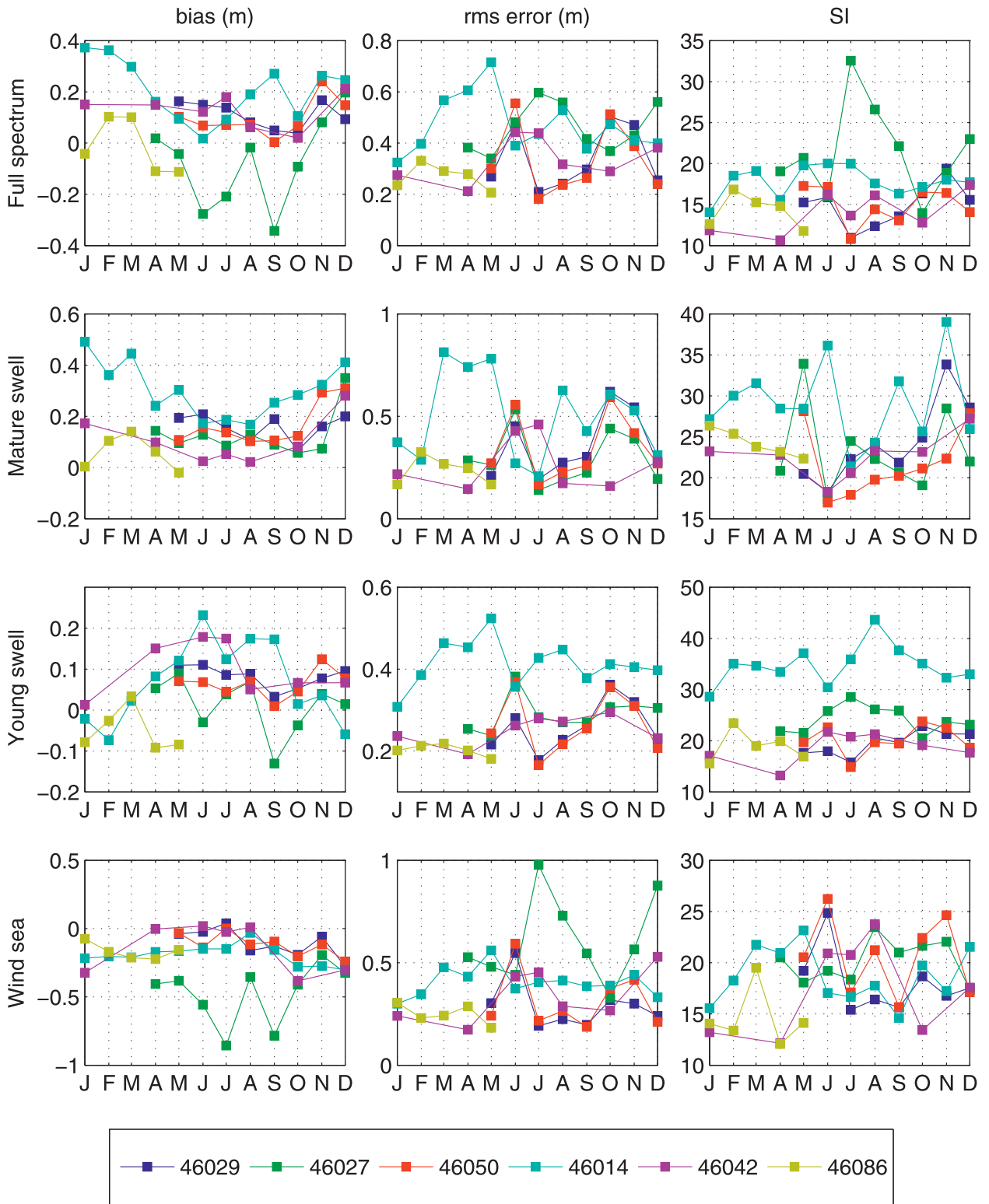


FIG. 13. Significant wave height error metrics from IMEDS for the Pacific buoys during 2008.

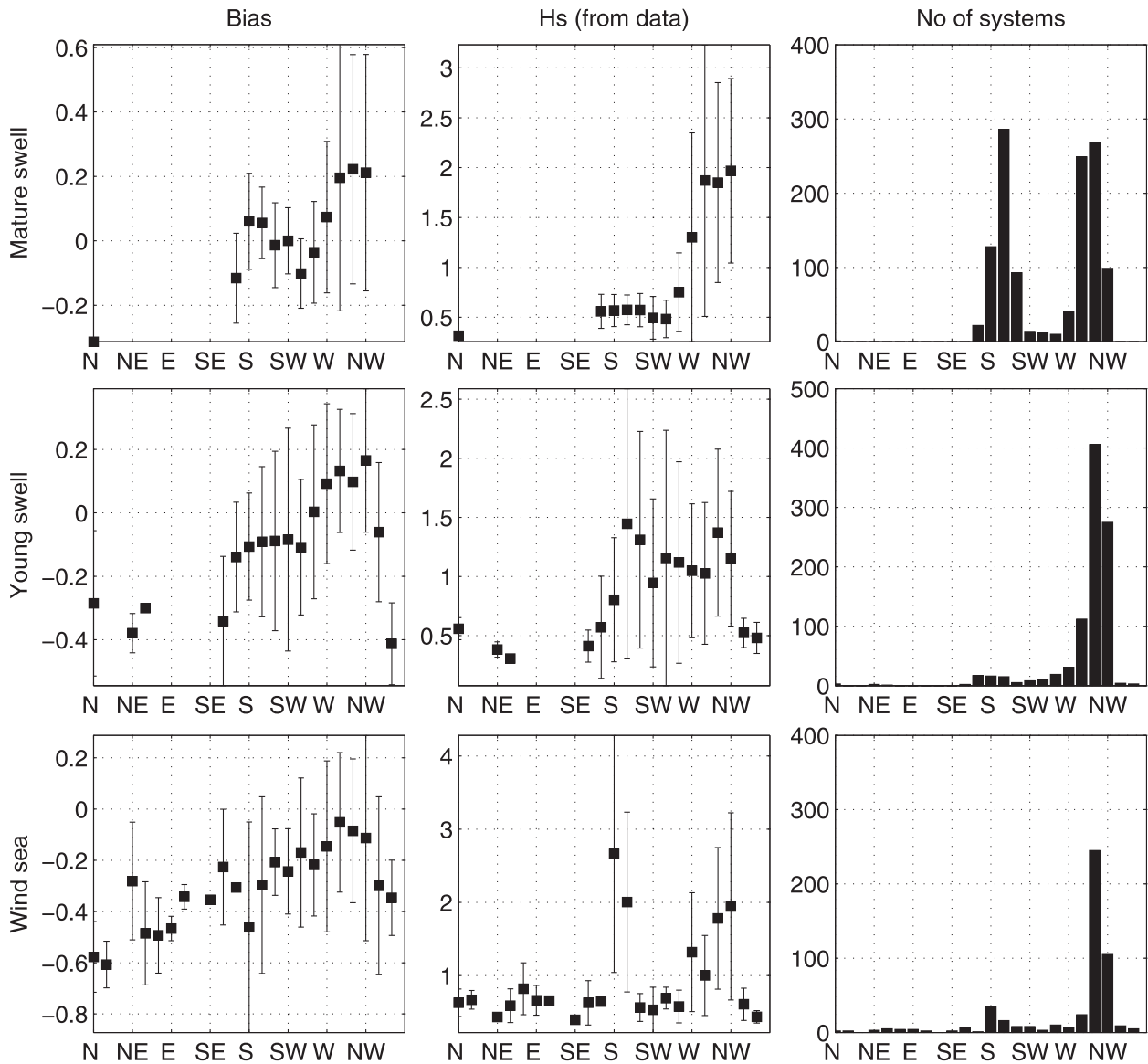


FIG. 14. As in Fig. 11, but for buoy 46042 in the Pacific Ocean.

prevalent winds, the overall impact of these interactions would be a net reduction in wave heights. Preliminary hindcast modeling studies by Hersbach and Bidlot (2009) have shown that including wave–current interactions can reduce wave heights by an order of 0.05–0.10 m in the vicinity of the ACC. While this is not enough to explain the observed wave biases in this region, this may be an important physical process and merits further investigation, but is beyond the scope of the present study.

**6. Conclusions**

With the development of the multigrid version of WW3, operational wave modeling at NCEP has moved

from a single-grid paradigm to a multigrid modeling system (implemented operationally on 27 November 2007). This approach provides the flexibility of having several different resolution grids (with the capability of having unique or common forcing fields) all exchanging wave information and being driven by a single model driver. In operations these grids are still regular latitude–longitude grids, but developments are currently under way to incorporate curvilinear as well as unstructured grids to have a truly flexible system where all these different grid types can be driven by a single model.

With the development of the new numerics, attention now shifts to the model physics that have not been changed in the NCEP operational model for over

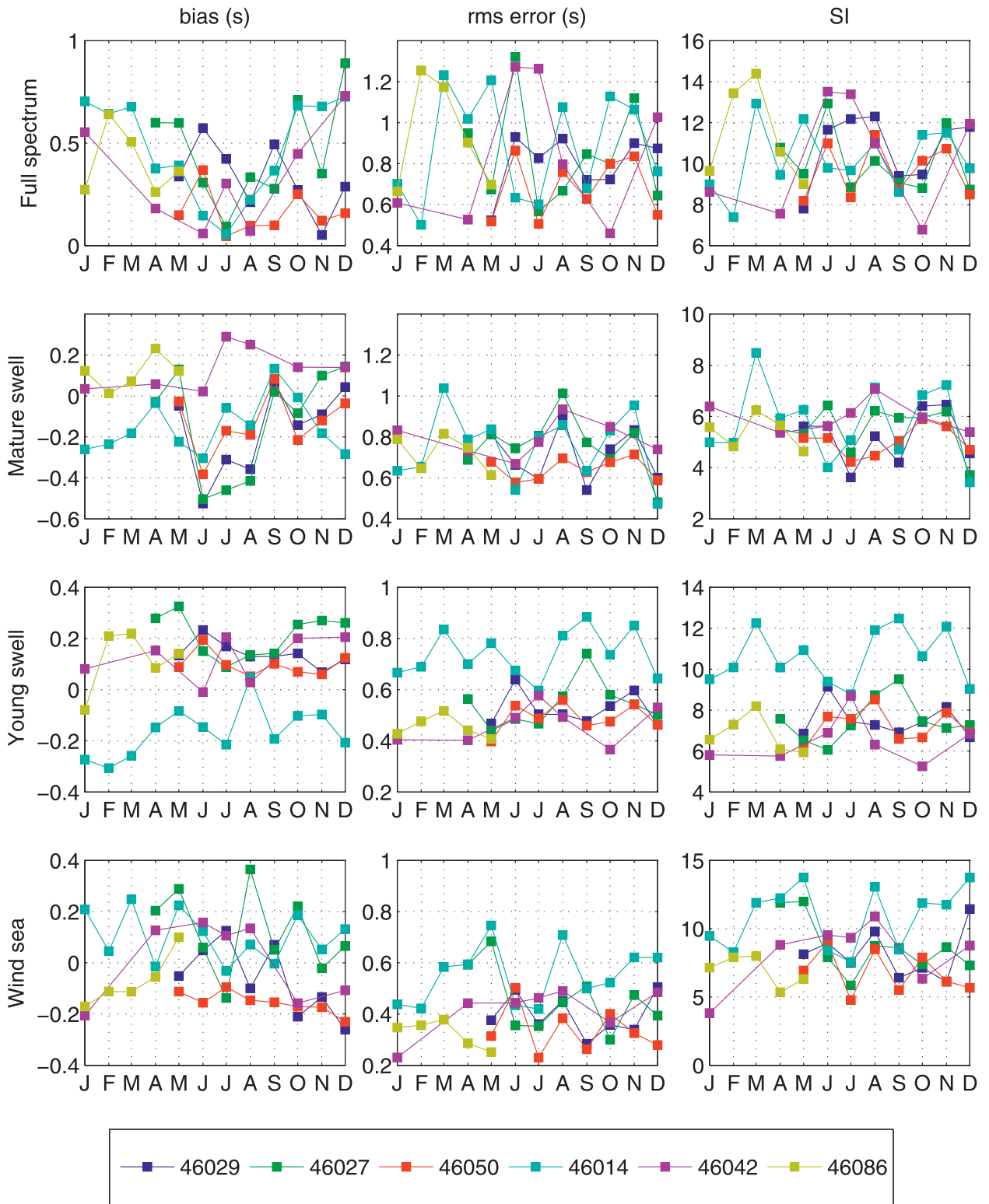


FIG. 15. Wave period error metrics from IMEDS for the Pacific buoys during 2008.

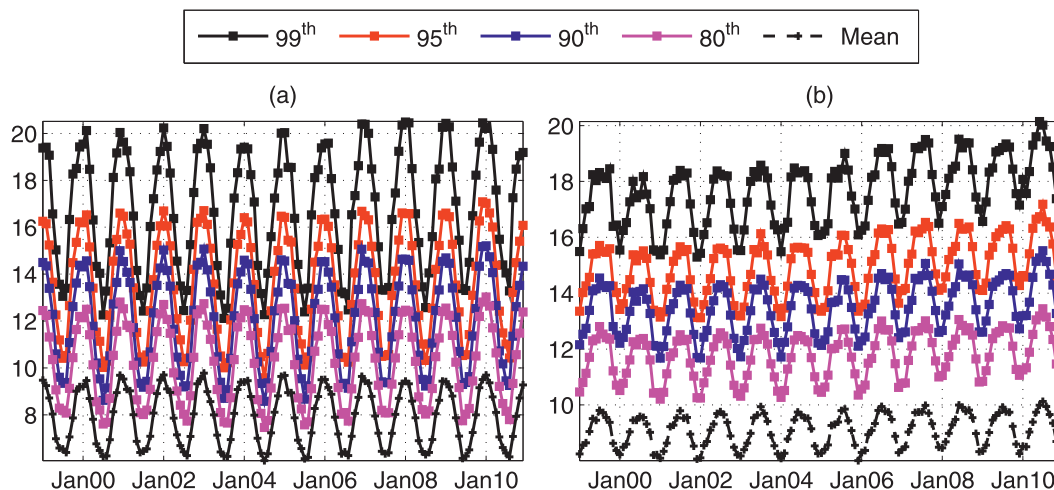


FIG. 16. Wind speed statistics (computed using month-long records) for the 10-m winds from the GFS model. Statistics have been computed separately for the (a) Northern Hemisphere defined from 25° to 60°N and (b) Southern Hemisphere defined from 60° to 25°S. All land points have been excluded. The y axis refers to wind speed ( $\text{m s}^{-1}$ ). The dashed line is the average speed, and the solid lines refer to the different percentiles of the wind speed distributions.

a decade. Validation studies have shown that while the skill scores are good, systemic errors in the model still remain. NCEP is participating in a multi-institutional 4-yr initiative through the National Oceanographic Partnership Program (NOPP) that has been assembled to improve wave physics in operational wind-wave models (Tolman et al. 2011). As part of this initiative, the first upgrade to operational wave modeling at NCEP is already under way<sup>4</sup> and further upgrades may be expected in the coming years.

*Acknowledgments.* The authors would like to acknowledge the efforts of Andre van der Westhuysen, Roberto Padilla, and Joseph Sienkiewicz at NCEP for their constructive comments on early drafts of this manuscript.

#### REFERENCES

- Ardhuin, F., T. H. C. Herbers, G. P. V. Vledder, K. P. Watts, R. Jensen, and H. C. Graber, 2007: Swell and slanting-fetch effects on wind wave growth. *J. Phys. Oceanogr.*, **37**, 908–931.
- , B. Chapron, and F. Collard, 2009: Observation of swell dissipation across oceans. *Geophys. Res. Lett.*, **36**, L06607, doi:10.1029/2008GL037030.
- , and Coauthors, 2010: Semiempirical dissipation source functions for ocean waves. Part I: Definition, calibration, and validation. *J. Phys. Oceanogr.*, **40**, 1917–1941.
- , J. Tournadre, P. Queffelec, F. Girard-Ardhuin, and F. Collard, 2011: Observation and parametrization of small icebergs: Drifting breakwaters in the Southern Ocean. *Ocean Modell.*, **39**, 405–410.
- Banner, M. L., and J.-B. Song, 2002: On determining the onset and strength of breaking for deep water waves. Part II: Influence of wind forcing and surface shear. *J. Phys. Oceanogr.*, **32**, 2559–2570.
- , and W. L. Peirson, 2007: Wave breaking onset and strength for two-dimensional deep water wave groups. *J. Fluid Mech.*, **585**, 93–115.
- , A. V. Babanin, and I. R. Young, 2000: Breaking probability for dominant waves on the sea surface. *J. Phys. Oceanogr.*, **30**, 3145–3160.
- Battjes, J. A., and J. P. F. M. Janssen, 1978: Energy loss and set-up due to breaking of random waves. *Proc. 16th Int. Conf. in Coastal Engineering*, Hamburg, Germany, American Society of Civil Engineers, 569–587.
- Bidlot, J., S. Abdalla, and P. Janssen, 2005: A revised formulation for ocean wave dissipation in Cy25r1. ECMWF Tech. Rep. R60.9/JB/0516, 35 pp.
- , P. Janssen, and S. Abdalla, 2007a: A revised formulation of ocean wave dissipation and its model impact. ECMWF Tech. Rep. 509, 29 pp.
- , and Coauthors, 2007b: Inter-comparison of operational wave forecasting systems. *10th Int. Workshop on Wave Hindcasting and Forecasting*, Oahu, HI, U.S. Army Engineer Research and Development Center/Coastal and Hydraulics Laboratory, 1–22.
- Booij, N., and L. H. Holthuijsen, 1987: Propagation of ocean waves in discrete spectral wave models. *J. Comput. Phys.*, **68**, 307–326.
- Caplan, P., J. Derber, W. Gemmill, S.-Y. Hong, H.-L. Pan, and D. Parrish, 1997: Changes to the 1995 NCEP operational Medium-Range Forecast model analysis-forecast system. *Wea. Forecasting*, **12**, 581–594.
- Cavaleri, L., and P. Malanotte-Rizzoli, 1981: Wind wave prediction in shallow water: Theory and applications. *J. Geophys. Res.*, **86** (C11), 10 961–10 973.

<sup>4</sup> Using the Ardhuin et al. (2010) physics, which went into operations in May 2012.

- Chalikov, D. V., and M. Belevich, 1993: One-dimensional theory of the wave boundary layer. *Bound.-Layer Meteor.*, **63**, 65–96.
- Chao, Y. Y., L. D. Burroughs, and H. L. Tolman, 2003a: Wave forecasting for Alaskan waters. NWS Tech. Procedures Bull. 496, 10 pp.
- , —, and —, 2003b: Wave forecasting for the eastern North Pacific and adjacent waters. NWS Tech. Procedures Bull. 491, NWS/NCEP, 11 pp.
- , —, and —, 2003c: Wave forecasting for the western North Atlantic Ocean and adjacent waters. NWS Tech. Procedures Bull. 459, NWS/NCEP, 11 pp.
- Chawla, A., and H. L. Tolman, 2007: Automated grid generation for WAVEWATCH III. NWS Tech. Note 254, 71 pp.
- , and —, 2008: Obstruction grids for spectral wave models. *Ocean Modell.*, **22**, 12–25.
- Derber, J. C., D. F. Parrish, and S. J. Lord, 1991: The new global operational analysis system at the National Meteorological Center. *Wea. Forecasting*, **6**, 538–547.
- Grumbine, R. W., 1996: Automated passive microwave sea ice concentration analysis at NCEP. NWS Tech. Note 120, 13 pp.
- Hanson, J. L., and R. E. Jensen, 2004: Wave system diagnostics for numerical wave models. *Eighth Int. Workshop on Wave Hindcasting and Forecasting*, Oahu, HI, Joint WMO–IOC Technical Commission for Oceanography and Marine Meteorology Tech. Rep. 29. [Available online at <ftp://ftp.wmo.int/Documents/PublicWeb/amp/mmop/documents/JCOMM-TR/J-TR-29-WH8/Papers/E3.pdf>.]
- , B. A. Tracy, H. L. Tolman, and R. D. Scott, 2009: Pacific hindcast performance of three numerical wave models. *J. Atmos. Oceanic Technol.*, **26**, 1614–1633.
- Hersbach, H., and J.-R. Bidlot, 2009: The relevance of ocean surface current in the ECMWF analysis and forecast system. *Proc. Workshop on Ocean–Atmosphere Interactions*, Reading, United Kingdom, ECMWF, 61–73.
- Janssen, P. A. E. M., 1991: Quasi-linear theory of wind wave generation applied to wave forecasting. *J. Phys. Oceanogr.*, **21**, 1631–1642.
- Kanamitsu, M., 1989: Description of the NMC global data assimilation and forecast system. *Wea. Forecasting*, **4**, 335–342.
- , and Coauthors, 1991: Recent changes implemented into the global forecast system at NMC. *Wea. Forecasting*, **6**, 425–435.
- Luetlich, R. A., J. Westerink, and N. Scheffner, 1992: ADCIRC: An advanced three-dimensional circulation model for shelves coasts and estuaries. Report 1: Theory and methodology of ADCIRC-2DDI and ADCIRC-3DL. Dredging Research Program Tech. Rep. DRP-92-6, U.S. Army Engineers Waterways Experiment Station, 137 pp.
- NOAA/NGDC, cited 2007: ETOPO2v2 global gridded 2-minute database. National Oceanic and Atmospheric Administration/ National Geophysical Data Center. [Available online at <http://www.ngdc.noaa.gov/mgg/global/etopo2.html>.]
- Reynolds, R. W., and T. M. Smith, 1994: Improved global sea surface temperature analyses, using optimum interpolation. *J. Climate*, **7**, 929–948.
- Rogers, W. E., 2002: The U.S. Navy’s global wind-wave models: An investigation into sources of errors in low-frequency energy predictions. Ocean Dynamics and Prediction Branch Tech. Rep. NRL/FR/7320-02-10,035, Naval Research Laboratory, 64 pp.
- Song, J.-B., and M. L. Banner, 2002: On determining the onset and strength of breaking for deep water waves. Part I: Unforced irrotational wave groups. *J. Phys. Oceanogr.*, **32**, 2541–2558.
- Tolman, H. L., 1992: Effects of numerics on the physics in a third-generation wind-wave model. *J. Phys. Oceanogr.*, **22**, 1095–1111.
- , 2002a: Distributed memory concepts in the wave model WAVEWATCH III. *Parallel Comput.*, **28**, 35–52.
- , 2002b: Testing of WAVEWATCH III version 2.22 in NCEP’s NWW3 ocean wave model suite. NWS Tech. Note 214, 99 pp.
- , 2002c: User manual and system documentation of WAVEWATCH III version 2.22. NWS Tech. Note 222, 133 pp.
- , 2002d: Validation of WAVEWATCH III version 1.15 for a global domain. NWS Tech. Note 213, 33 pp.
- , 2003: Treatment of unresolved islands and ice in wind wave models. *Ocean Modell.*, **5**, 219–231.
- , 2007: Development of a multi-grid version of WAVEWATCH III. NOAA/NWS/NCEP/MMAB Tech. Note 256, 88 pp.
- , 2008: A mosaic approach to wind wave modeling. *Ocean Modell.*, **25**, 35–47.
- , 2009: User manual and documentation of WAVEWATCH III version 3.14. NOAA/NWS/NCEP/MMAB Tech. Note 276, 219 pp.
- , and D. Chalikov, 1996: Source terms in a third-generation wind wave model. *J. Phys. Oceanogr.*, **26**, 2497–2518.
- , B. Balasubramanian, L. D. Burroughs, D. V. Chalikov, Y. Y. Chao, H. S. Chen, and V. M. Gerald, 2002: Development and implementation of wind-generated ocean surface wave models at NCEP. *Wea. Forecasting*, **17**, 311–333.
- , D. Cao, and V. M. Gerald, 2006: Altimeter data for use in wave models at NCEP. NWS Tech. Rep. 252, 49 pp.
- , M. L. Banner, and J. M. Kaihatu, 2011: The NOPP operational wave model improvement project. *12th Int. Workshop on Wave Hindcasting and Forecasting/3rd Coastal Hazards Symp.*, Waikoloa, HI, Environment Canada–U.S. Army Engineer Research and Development Center’s Coastal and Hydraulics Laboratory, I12.
- Vincent, L., and P. Soille, 1991: Watersheds in digital spaces: An efficient algorithm based on immersion simulations. *IEEE Trans. Pattern Anal. Mach. Intell.*, **13**, 583–598.
- Wessel, P., and W. Smith, 1996: A global, self-consistent, hierarchical, high-resolution shoreline database. *J. Geophys. Res.*, **101** (B4), 8741–8743.
- Young, I. R., and A. V. Babanin, 2006: Spectral distribution of energy dissipation of wind-generated waves due to dominant wave breaking. *J. Phys. Oceanogr.*, **36**, 376–394.